https://doi.org/10.1016/j.ijrmhm.2016.11.006

Application of X- ray diffraction to study the grinding induced surface damage mechanism of WC/Co

Quanli Zhang[1,2], Qingliang Zhao[1*], Suet To[2] and Bing Guo[1]

[1] Centre for Precision Engineering, School of Mechatronics Engineering, Harbin Institute of Technology, Harbin, 150001, China

[2] State Key Laboratory of Ultra-precision Machining Technology, The Hong Kong Polytechnic University, Hong Kong

*Corresponding Author / E-mail: zhaoqingliang@hit.edu.cn, TEL: +86-451 8640 2683, FAX: +86-451 8641 5244

Abstract

X-ray diffraction was utilized to examine the WC/Co surface after high spindle speed grinding (HSSG) to get a further insight into the machining induced surface damage mechanism. The results showed that grinding induced reorientation and preferred {100}/{10-10} growth of WC particles occurred in the deformed surface, while the crystallinity of WC(001) increased. Based on the analysis of the penetration depth of X ray in WC and Co, grazing incidence X-ray diffraction (GIXRD) showed that the grinding induced preferred crystal growth occurred only in the outmost layer (~3.324 nm), but the compressive stress was caused to a certain depth of the subsurface (>756.18 nm).

Keywords: X-ray diffraction; Preferred orientation; Compressive stress; WC/Co; Grinding

1. Introduction

Grinding of cemented carbides has been widely conducted for the extensive application of WC/Co in molding industry, automatic field and cutting tools [1-5]. To improve the life span of the devices or tools, the (sub-)surface damage induced during the machining is of great concern. It has been reported that the varied worn modes occurred for the machined surface, such as surface deformation, fracture, grain pull-outs, and residual stress [3, 5-7].

To characterize the surface damages, different methods have been applied to examine the machined surface, such as Electron Backscattering Diffraction (EBSD) [7, 8], Transmission Electron Microscope (TEM) [9-12], Scanning Electron Microscope (SEM) equipped with Energy Dispersive Spectra (EDS), Focused Ion Beam (FIB) [6], as well as X-ray Diffraction (XRD) [1, 13, 14]. In comparison, X ray diffraction (XRD) technique provides us an effective and nondestructive approach to detect the structure transformation of the machined surface.

In the present work, XRD (Bragg-Brentano X-ray diffraction and Grazing incidence X-ray diffraction) is utilized to characterize the grinding induced crystallinity change and preferred orientation of WC/Co, and the corresponding theoretical analysis is given based on the specific crystal structure of WC.

2. Experiments

High spindle speed grinding (HSSG) of WC/Co (~10 wt.%Co) composites was conducted on an ultra-precision grinding machine (Moore Nanotech 450UPL, USA), with minimum quantity of oil coolant (CLAISOL 350). Detail information of the materials properties and grinding setup could be found in our previous studies [5, 15]. The micro-structure change of the machined WC/Co surface was characterized by Bragg-Brentano X-ray diffraction (BBXRD) and Grazing

Incidence X-ray diffraction (GIXRD) with CuK_α radiation (Rigaku SmartLab) in a scanning angle range of 20 to 80°. The spectra was analyzed by Jade 6.5, compared with the standard PDF2-2004 database, and the reference number of the powder diffraction file for WC is PDF#73-471.

3. Results and discussion

To eliminate the impact of the rough surface after sintering, the WC/Co was firstly polished with the diamond paste of 1 μm diameter to remove the surface layer and reduce the impact of the surface defects. The surface morphology, as shown in Fig. 1(a), of the polished WC/Co composites indicates that there are no obvious defects in the original bulk material and the average grain size of WC is about 2 μm. The obtained surface roughness (R_a, arithmetic mean of the departures of the profile) was about 3 nm for the workpiece after polishing, as shown in Fig. 1(b). Fig. 1(c) and Fig. 1(d) shows the surface morphology and surface topography of WC/Co after grinding. It can be readily seen that the machined surface is covered by scratching grooves, WC grain dislodgement, as well as the extrusion of binder. In addition, the surface roughness reached 5.43 nm (R_a). Compared with the original surface, the XRD pattern of the machined surface, as shown in Fig. 2, shows some reduction in the peak intensity, which is firstly attributed to the formation of a densified layer that is seriously deformed under the dynamic pressure of diamond grits [16]. Specifically, due to the extrusion of cobalt binder, the surface deformation was induced during grinding, where the mean free path of WC grains decreased, resulting in the densification of the deformed surface [1, 14, 15]. In addition, amorphization of WC could be induced under the shear stress of the dynamic diamond grits during grinding, which has been reported by Stoyanov et al [17], and this could also lead to the decreasing peak intensity.

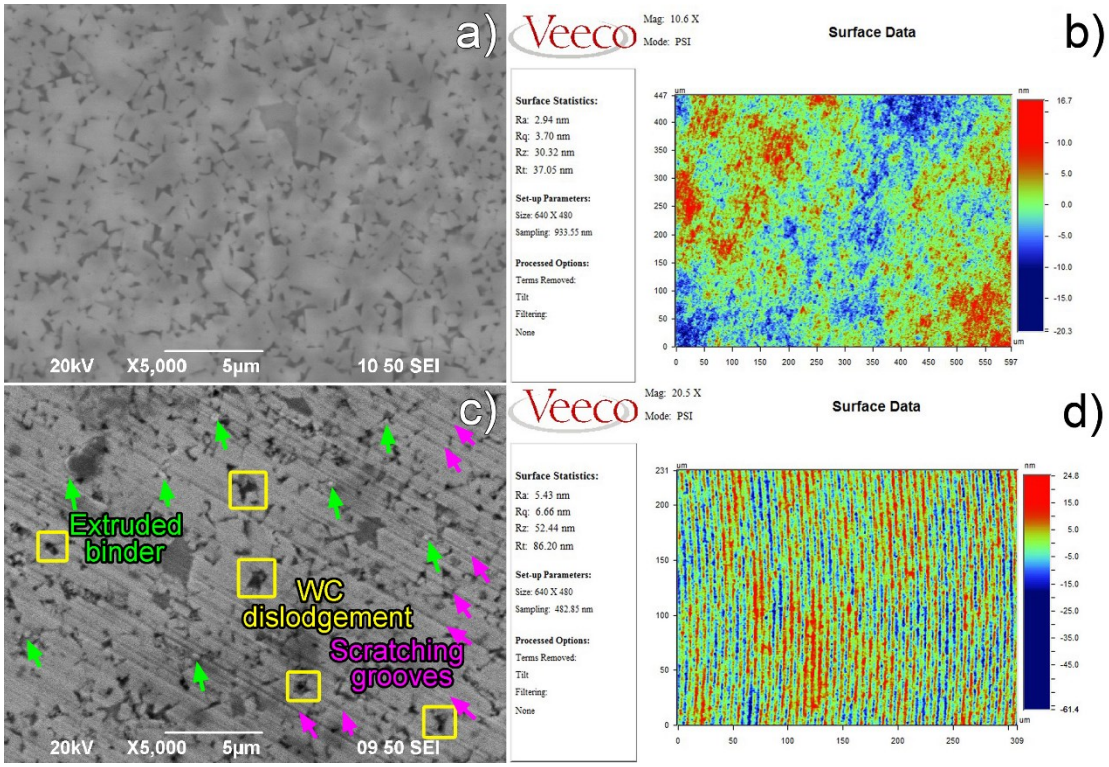

Fig. 1 Surface morphology and topography of WC/Co after polishing and grinding: (a) and (b) after polishing, (c) and (d) after grinding

Crystallinity is specified as a percentage of the volume of the material that is crystalline, and the crystallinity of the different crystal planes for WC is calculated by Eq. (1):

$$Crystallinity = I_{\text{Intensity of crystalline peaks}} / I_{\text{Total intensity of spectrum}} \times 100\% \quad (1)$$

In the present work, the calculated crystallinity of WC, as shown in Fig. 2(c), indicated that the crystallinity for WC(001), WC(100) and WC(101) all decreased, and this is attributed to the formation of amorphous WC [17]. In addition, the texture coefficient of different crystal planes for WC could also be obtained referring to [18, 19], which was calculated based on Eq. (2),

$$T_c = \frac{n I_{hkl} / I^0_{hkl}}{\sum I_{hkl} / I^0_{hkl}} \quad (2)$$

where I_{hkl} is the measured peak intensity of (hkl) plane, I^0_{hkl} is the peak intensity of the same plane as indicated in the standard sample (PDF#73-471), n is the total number of reflections observed

(n=3). Based on the crystal structure of WC, as shown in Fig. 2(e), it can be easily seen that the close-packed crystal plane is {0001}, and the close-packed orientation is <-12-10>. To low the system energy, preferred WC{0001}/<-12-10> growth is expected during sintering, so the preferred orientation for the original workpiece is WC(001), as shown in Fig. 2(d).

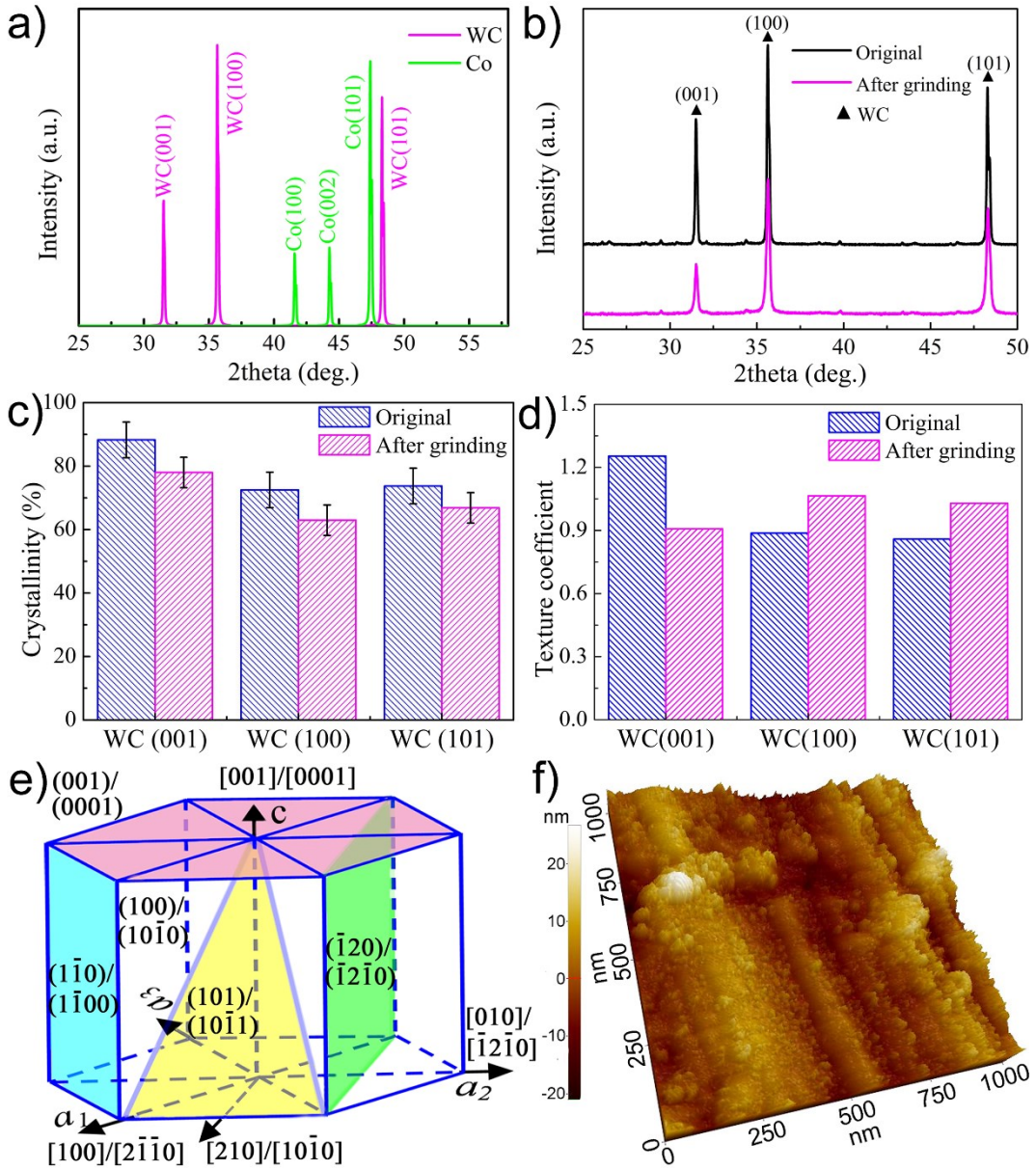

Fig. 2 (a) Standard XRD pattern for WC and Co phases, (b) XRD pattern of the original material and machined surface, (c) the calculated crystallinity of the original and machined WC/Co, (d) the calculated texture coefficient, (e) typical crystal plane and orientation of WC, (f) surface

topography of the machined WC/Co measured by AFM

However, the preferred orientation of WC(100)/(10-10) appeared for the machined surface, as indicated in Fig. 2(d). As far as the high grinding temperature and dynamic pressure of the diamond grits were concerned, the grain growth of WC could be induced, which promoted the further growth of WC grains, leading to the preferred growth of WC(100)/(10-10) for the machined surface. The surface topography of the machined WC/Co measured by AFM in a range of 1 μm×1 μm is shown in Fig. 2(f). It can be readily seen that the machined surface is covered by many nano grains. According to the previous experimental and theoretical study, the instantaneous temperature of the grinding zone, which is called 'spike' or 'flash' temperature, could be close to the melting point of the workpiece material with minimum quantity lubrication, especially at a very small depth of cut where the friction heats resulted in the high temperature [20-22]. Therefore, the preferred growth for the nano grains could be induced during the grinding process under this consideration.

Previous studies have also shown that reorientation of grains could be induced in the seriously deformed layer [23-25], and the reaction indicated by Eq. (3) occurred [26]. In addition, a tendency of fracture path occurred on {10-10} has been proposed during the indentation of WC/Co [27]. Therefore, the expected orientation alignment and grain fracture could lead to the increasing amount of prismatic planes (WC{100}/{10-10}), resulting in the preferred WC(100)/(10-10).

$$\frac{1}{6}\left[11\bar{2}\bar{3}\right]\left(\bar{1}100\right)+\frac{1}{6}\left[2\bar{1}\,\bar{1}3\right]\rightarrow\frac{1}{2}\left[10\bar{1}0\right] \tag{3}$$

As is known, the machined surface of WC/Co after grinding is always covered by a deformed layer of about 2 μm or more [23-25], and it could be seen as a thin film. Compared to BBXRD,

the outmost layer could be characterized by GIXRD with a controlled incident angle [28-30]. Fig. 3 shows the XRD instrument and the schematic of GIXRD geometry performed in out of plane mode. A critical incident angle α_c is believed to be of great significance for GIXRD and it could be determined by Eq. (4) [30],

$$\alpha_c = \sqrt{2 \times \frac{N_A r_e \rho}{2\pi A} \lambda^2 \left(f_0 + f'\right)} = \sqrt{\frac{N_A r_e \rho Z}{\pi A} \lambda} \tag{4}$$

where α_c is the critical incidence angle, α_i is the incidence angle, r_e is the classical electron radius, N_A is the Avogadro constant, A is the mean atomic weight, ρ is the mass density, λ the wavelength of X ray, f_0 is the atomic scattering factor, f' is the dispersion correction term for f_0, Z is the atomic number of workpiece. Based on Eq. (4), the critical incident angle for WC and Co was achieved to be 0.5181° and 0.414°. When the incident angle is less than the critical angle ($\alpha_i < \alpha_c$), the total external reflection of X ray would occur and the penetration depth is limited to the outmost surface layer; if $\alpha_i \geq \alpha_c$, the depth of penetration would rise rapidly, as illustrated by Eq. (5) and Eq. (6) [30].

$$L = \frac{\lambda}{2\pi\sqrt{\alpha_c^2 - \sin^2 \alpha_i}}, \quad \alpha_i < \alpha_c \tag{5}$$

$$L = \frac{1}{2\mu} \cdot \sin\alpha_i, \quad \alpha_i \geq \alpha_c \tag{6}$$

where L is the penetration depth and μ is the linear absorption coefficient. Therefore, GIXRD could serve as an effective tool in the study of subsurface damage, including phase structure and residual stress.

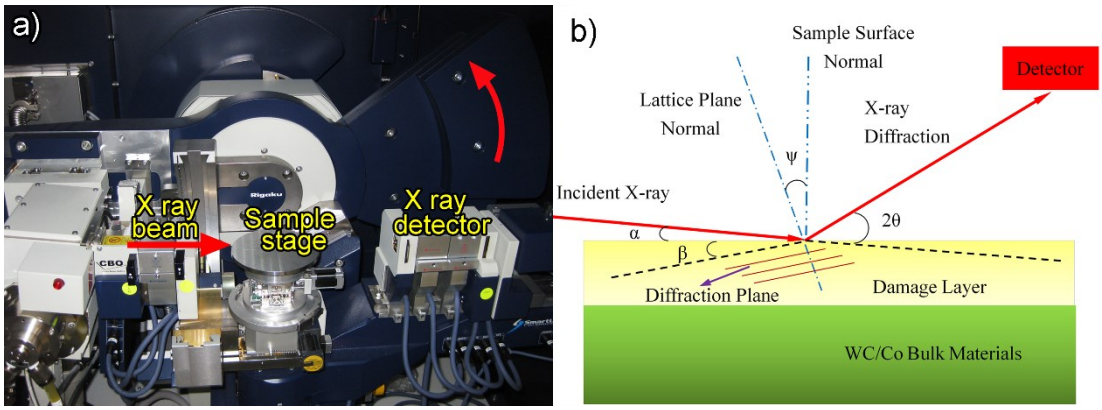

Fig. 3 (a) Illustration of the XRD instrument, (b) schematic of the GIXRD geometry for out of plane mode, where the damage layer is assumed to be a thin film isolated from bulk material

As shown in Fig. 4(a), the peak intensity grows stronger with the increasing incident angle. Specifically, compared with the standard peak position (PDF#73-471), the peak position of the machined surface shows some right shift, indicating the decreasing crystal space and compressive stress, as shown in Fig .4(b), and the compressive stress exists to some depth beneath the grinding surface, which is greater than 756.18 nm (the calculated penetration depth of X ray at α_i=1.2° by Eq. (6)). In addition, the texture coefficient for the outmost layer, the depth of which is calculated to be 3.324 nm at the incident angle of 0.3° based on Eq. (5), obviously differs with the subsurface over a certain depth, where preferred orientation of WC(100)/(10-10) appears. However, the further increase of incident angle shows that the texture coefficient does not change obviously, which indicates that the grinding induced preferred crystal growth occurred only in the outmost layer.

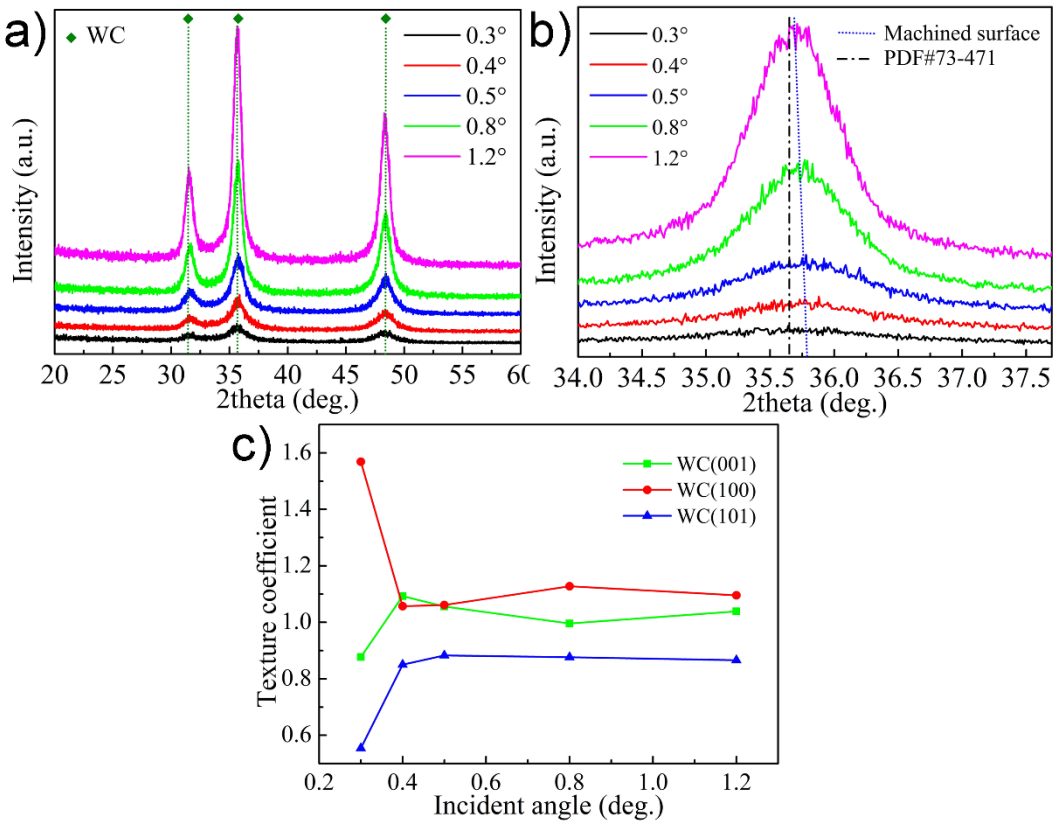

Fig. 4 (a) GIXRD pattern of the machined surface at different incident angle, (b) an enlarged view around the peak of WC(100, (c) the calculated texture coefficient for WC(001), WC(100) and WC(101)

4. Conclusions

X ray diffraction is applied to examine the grinding WC/Co surface in the present work. The results showed that the preferred WC{100}/{10-10} growth occurred in the outmost surface (~3.324 nm), which is in good consistence with the theoretical analysis based on the crystal structure of WC. In addition, compressive stress was induced to some depth (>756.18 nm) during grinding.

Acknowledgements

The authors are grateful for the financial support from the National Natural Science Foundation of China (NSFC) (Project No.:51475109) and also the Research Committee of the

Hong Kong Polytechnic University (RTRA).

References

[1] J.B.J.W. Hegeman, J.T.M. De Hosson, G. de With, Grinding of WC-Co hardmetals, Wear 248 (2001) 187-196.

[2] R. Morrell, A.J. Gant, Edge chipping of hard materials, International Journal of Refractory Metals and Hard Materials 19 (2001) 293-301.

[3] A.J. Gant, M.G. Gee, B. Roebuck, Rotating wheel abrasion of WC/Co hardmetals, Wear 258 (2005) 178-188.

[4] Q. Zhang, S. To, Q. Zhao, B. Guo, Surface generation mechanism of WC/Co and RB-SiC/Si composites under high spindle speed grinding (HSSG), International Journal of Refractory Metals and Hard Materials 56 (2016) 123-131.

[5] Q. Zhang, S. To, Q. Zhao, B. Guo, G. Zhang, Impact of material microstructure and diamond grit wear on surface finish in micro-grinding of RB-SiC/Si and WC/Co carbides, International Journal of Refractory Metals and Hard Materials 51 (2015) 258-263.

[6] A.J. Gant, M.G. Gee, D.D. Gohil, H.G. Jones, L.P. Orkney, Use of FIB/SEM to assess the tribo-corrosion of WC/Co hardmetals in model single point abrasion experiments, Tribology International 68 (2013) 56-66.

[7] M. Gee, K. Mingard, B. Roebuck, Application of EBSD to the evaluation of plastic deformation in the mechanical testing of WC/Co hardmetal, International Journal of Refractory Metals and Hard Materials 27 (2009) 300-312.

[8] K.P. Mingard, M.G. Gee, EBSD examination of worn WC/Co hardmetal surfaces, Wear 263 (2007) 643-652.

[9] C.H. Vasel, A.D. Krawitz, E.F. Drake, E.A. Kenik, Binder deformation in WC-(Co, Ni) cemented carbide composites, Metallurgical Transactions A 16 (1985) 2309-2317.

[10] V.K. Sarin, T. Johannesson, On the deformation of WC-Co cemented carbides, Metal Science 9 (1975) 472-476.

[11] U. Schleinkofer, H.G. Sockel, K. Go Rting, W. Heinrich, Microstructural processes during subcritical crack growth in hard metals and cermets under cyclic loads, Materials Science and Engineering: A 209 (1996) 103-110.

[12] A. Duszová, P. Hvizdoš, F. Lofaj, Ł. Major, J. Dusza, J. Morgiel, Indentation fatigue of WC-Co cemented carbides, International Journal of Refractory Metals and Hard Materials 41 (2013) 229-235.

[13] C. Larsson, M. Odén, X-ray diffraction determination of residual stresses in functionally graded WC-Co composites, International Journal of Refractory Metals and Hard Materials 22 (2004) 177-184.

[14] J. Yang, M. Odén, M.P. Johansson-Jõesaar, L. Llanes, Grinding effects on surface integrity and mechanical Strength of WC-Co Cemented Carbides, Procedia CIRP 13 (2014) 257-263.

[15] Q. Zhang, S. To, Q. Zhao, B. Guo, M. Wu, Effects of binder addition on the surface generation mechanism of WC/Co during high spindle speed grinding (HSSG), International Journal of Refractory Metals and Hard Materials 59 (2016) 32-39.

[16] Y. Waseda, E. Matsubara, K. Shinoda, X-Ray Diffraction Crystallography: Introduction, Examples and Solved Problems, Springer, 2011.

[17] P. Stoyanov, P.A. Romero, T.T. Järvi, L. Pastewka, M. Scherge, P. Stemmer, A. Fischer, M. Dienwiebel, M. Moseler, Experimental and numerical atomistic investigation of the third

body formation process in dry tungsten/tungsten-carbide tribo couples, Tribology Letters 50 (2013) 67-80.

[18] S. Mukherjee, F. Prokert, E. Richter, W. Moeller, Compressive stress, preferred orientation and film composition in Ti-based coatings developed by plasma immersion ion implantation-assisted deposition, Surface and Coatings Technology 186 (2004) 99-103.

[19] M.I. Jones, I.R. McColl, D.M. Grant, Effect of substrate preparation and deposition conditions on the preferred orientation of TiN coatings deposited by RF reactive sputtering, Surface and Coatings Technology 132 (2000) 143-151.

[20] S. Malkin, C. Guo, Grinding technology: theory and applications of machining with abrasives, New York: Industrial Press, 2008..

[21] S. Malkin, C. Guo, Thermal analysis of grinding, CIRP Annals - Manufacturing Technology 56 (2007) 760-782.

[22] B.V. Tanikella, A.H. Somasekhar, A.T. Sowers, R.J. Nemanich, R.O. Scattergood, Phase transformations during microcutting tests on silicon, Applied Physics Letters 69 (1996) 2870-2872.

[23] V. Kumar, Z.Z. Fang, S.I. Wright, M.M. Nowell, An analysis of grain boundaries and grain growth in cemented tungsten carbide using orientation imaging microscopy, Metallurgical and Materials Transactions A 37 (2006) 599-607.

[24] M. Pellan, S. Lay, J. Missiaen, S. Norgren, J. Angseryd, E. Coronel, T. Persson, Effect of binder composition on WC grain growth in cemented carbides, Journal of the American Ceramic Society 98 (2015) 3596-3601.

[25] X. Yuan, G.S. Rohrer, X. Song, H. Chien, J. Li, C. Wei, Effect of plastic deformation on the

Σ2 grain boundary plane distribution in WC-Co cemented carbides, International Journal of Refractory Metals and Hard Materials 47 (2014) 38-43.

[26] M. Bľanda, A. Duszová, T. Csanádi, P. Hvizdoš, F. Lofaj, J. Dusza, Indentation hardness and fatigue of the constituents of WC-Co composites, International Journal of Refractory Metals and Hard Materials 49 (2015) 178-183.

[27] K.P. Mingard, H.G. Jones, M.G. Gee, B. Roebuck, J.W. Nunn, In situ observation of crack growth in a WC-Co hardmetal and characterisation of crack growth morphologies by EBSD, International Journal of Refractory Metals and Hard Materials 36 (2013) 136-142.

[28] C.E. Murray, Origin of stress gradients induced in capped, copper metallization, Applied Physics Letters 104 (2014) 81920.

[29] B.W. Batterman, D.C. Wack, H. Dosch, Depth-controlled grazing-incidence diffraction of synchrotron X radiation, Physical Review Letters 56 (1986) 1144-1147.

[30] H. Dosch, Evanescent absorption in kinematic surface Bragg diffraction, Physical Review B 35 (1987) 2137-2143.